Journal of Materials Chemistry A

Grafting conductive polymers on graphene oxide through cross-linker: a stepwise approach

Journal:	*Journal of Materials Chemistry A*
Manuscript ID	TA-ART-05-2020-005489.R1
Article Type:	Paper
Date Submitted by the Author:	23-Jun-2020
Complete List of Authors:	Khan, Rizwan; Okayama University Nishina, Yuta; Okayama University, Research Core for Interdisciplinary Sciences

ARTICLE

Grafting conductive polymers on graphene oxide through cross-linker: a stepwise approach

Received 00th January 20xx,
Accepted 00th January 20xx

DOI: 10.1039/x0xx00000x

Rizwan Khan[a] and Yuta Nishina*[a,b]

A three-step reaction furnished a composite of graphene and a conductive polymer. In the first step, graphene oxide was modified with a diamine, which acted as a linker for polymer attachment. In the second step, an initiating site was attached to the free amine of the linker. Finally, a polymer was grown from the initiation site, and graphene oxide was reduced during polymer growth. The method does not require any catalyst, acid, or reducing agent, furnishing the graphene–polymer composite in a straightforward procedure. Various instrumental techniques, including step-by-step AFM analysis, were used to characterize the structure of the products in each step and confirm the covalent functionalization among graphene oxide, cross-linker, and polymer. The average surface height was sequentially increased after each step, indicating the success of the sequential reactions. The graphene-polymer composite showed excellent electrochemical performance and stability compared with a composite prepared by physical mixing of graphene and polymer.

Introduction

Among the many proposed applications of graphene-based materials, supercapacitors, also known as electrochemical capacitors, have been an active area of research for the past decade [1–3]. Compared with secondary batteries, graphene-based supercapacitors are electrochemical energy storage devices that promise outstanding power density [4], charge/discharge rate [5], cycling stability [6], and operational safety [7]. Supercapacitors are often utilized individually or in tandem with batteries for energy storage and supply (Scheme 1ai). They can be classified into two types: the electric double-layer capacitor (EDLC) (Scheme 1aii) and the pseudocapacitor (Scheme 1aiii). The energy storage mechanism of the EDLC involves a simple charge separation at the interface between the conductive electrode and the electrolyte. Because there is no chemical transformation at the EDLC electrodes, the system is quite stable, although the specific capacitance is relatively low [8,9]. In comparison, charge storage in a pseudocapacitor is predominantly achieved via the redox or faradic transformation of capacitive electrode materials, such as metal oxides [10] and conductive polymers [11]. The specific capacitance of the pseudocapacitor is generally high, but gradually decays because of structural collapse and degradation. A composite of a conductive substance and a pseudocapacitive material is desirable to enhance the overall capacitance, charge/discharge rate, and cycling lifetime. Graphene is a promising conductive component because it has a large surface area [12-14], and excellent electronic [15,16] and mechanical properties [17,18]. To develop a high-performance pseudocapacitor, we focused on developing a conductive polymer as an electrode counterpart to graphene. Various graphene–polymer composites with non-covalent and covalent interactions have been synthesized, and high capacitive performances have been achieved. The non-covalent interaction between graphene and polymers limits charge transfer at their interface, and hence constrains the cycling stability (Scheme 1bi) [19]. To address this issue, we propose the formation of the covalent bond between graphene and redox-active polymers.

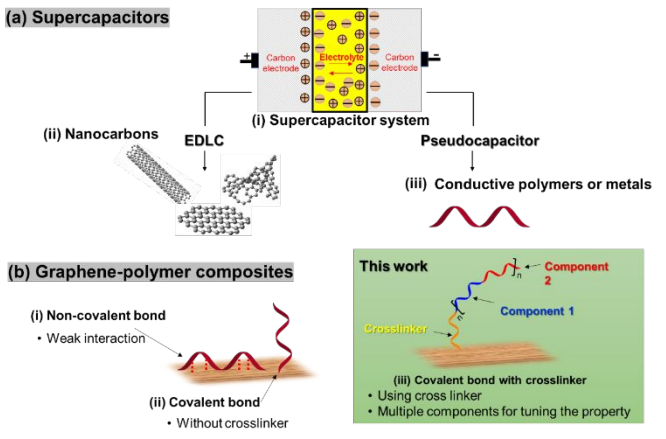

Scheme 1. (a) (i) Supercapacitor systems, (ii) EDLC-type carbon materials, and (iii) pseudocapacitor-type conductive polymer or metals. (b) Synthesis of graphene-polymer through (i) non-covalent bond, (ii) covalent bond, and (iii) present work: covalent bond with cross-linker.

Liu covalently functionalized graphene using amidation to graft phenylenediamine to chlorinated graphene oxide (GO), followed by polymerization and reduction [20]. Gao [21], Baek

[a] Graduate school of natural science and technology, Okayama University, 3-1-1 Tsushimanaka, Kita-ku, Okayama 700-8530, Japan.
[b] Research Core for Interdisciplinary Sciences, Okayama University, 3-1-1 Tsushimanaka, Kita-ku, Okayama 700-8530, Japan.
† Footnotes relating to the title and/or authors should appear here.
Electronic Supplementary Information (ESI) available: [details of any supplementary information available should be included here]. See DOI: 10.1039/x0xx00000x

[22], Liu [23], and Shen [24], independently reported the covalent grafting of polyaniline to graphene; all these methods initially functionalized graphene with phenylenediamine, then added aniline to initiate polymerization under acidic and oxidative conditions. As a result, a covalently cross-linked graphene–polymer composite was formed (Scheme 1bii). Herein, we synthesized a new type of composite containing a linker between the polymer and graphene (Scheme 1biii). The graphene–polymer composite was synthesized using a three-step reaction involving a cross-linker, initiator, and monomer. The prepared polymer–graphene composite was used as an electrode material for a supercapacitor.

Experimental

Materials

Natural graphite fakes (99.8%) were obtained from Alfa Aesar. *p*-Phenylenediamine, *m*-phenylenediamine, and 1,3-diaminopropane were obtained from Tokyo Chemical Industry Co., Ltd. Potassium permanganate ($KMnO_4$), sulfuric acid (H_2SO_4, 96%), thionyl chloride ($SOCl_2$), dimethylformamide (DMF), and ethanol were obtained from FUJIFILM Wako Pure Chemical Corporation and used as received

Synthesis of graphene oxide (GO)

Natural graphite (100 g) was dispersed into concentrated H_2SO_4 (2.5 L). After cooling the mixture in an ice bath, $KMnO_4$ (300 g) was added while the reaction mixture was kept below 55°C. The mixture was stirred at 35°C for 2 h to complete the oxidation. Next, deionized water (2.5 L) was added slowly, and the temperature was kept below 50°C with continuous stirring, followed by the addition of H_2O_2 (30% aq., 250 mL) into the mixture. Finally, the brown crude graphite oxide was purified by performing 10 times centrifugation, and graphene oxide (GO) was prepared. The concentration of GO was measured by drying the GO dispersion under vacuum at 50°C overnight.

Preparation of *N,N*-bissulphinyl-*m*-benzenediamine (m-monomer)

m-Phenylenediamine (0.5 g) was taken in a 250 mL round-bottomed flask fitted with a dropping funnel containing thermometer. The flask was kept in an ice-bath, and $SOCl_2$ (1 mL) was added dropwise to *m*-phenylenediamine such that the reaction temperature was kept below 0°C. The flask was taken out from the ice bath and allowed to attain room temperature. Then, the reaction mixture was refluxed for 8 h at 80°C. The reaction mixture was filtered, washed with benzene, and dried under vacuum [25].

Synthesis of GO 1

In a typical procedure, 1,3-diaminopropane (0.5 mL) was added dropwise to the suspension of GO (250 mg L^{-1}, 400 mL) under vigorous stirring in a flask. The resulting mixture was allowed to stir for 24 h at room temperature, then filtered and thoroughly washed with ethanol and water several times. The obtained solid was freeze-dried for two days.

Synthesis of GO 2

In a typical procedure, the dispersion of **GO 1** (140 mg) was prepared in DMF (50 mL). Then *m*-monomer (140 mg) was added to the **GO 1** dispersion, and the mixture was sonicated for 1 h. The mixture solution was refluxed at 160°C for 24 h in an oil bath. After completion of the reaction, the mixture solution was filtered, and the solid product was washed with DMF and water several times. The product was then dried under vacuum for two days.

Synthesis of GO 3

In a typical procedure, *m*-monomer (140 mg) was added into a dispersion of **GO 1** (140 mg) in DMF (50 mL) and sonicated for 1 h. Then the reaction mixture was refluxed at 160°C for 24 h in an oil bath to obtain **GO 2**. To this mixture, *p*-phenylenediamine (140 mg) was added and refluxed at 180°C for another 36 h. After completion of the reaction, the reaction mixture was filtered, and the solid product was washed with DMF and water several times. The final product was then dried under vacuum for two days to obtained **GO 3**.

Structural characterization

The thermogravimetry analysis (TGA, RIGAKU TG 8121) was measured at a heating rate of 10°C min^{-1} from room temperature to 900°C under a nitrogen atmosphere. Fourier transform-infrared (FT-IR, SHIMADZU IR Tracer-100) were recorded in the range of 500-4000 cm^{-1}. The samples for FT-IR analysis were dried and mixed with KBr, and then pressed into 1.3 mm-diameter pellets. The morphologies of the composite were characterized using a scanning electron microscope (SEM, HITACHI S-5200) and atomic force microscopy (AFM, SHIMADZU SPM-9700HT). Images were obtained through the deposition of the dispersions on oxidized Si wafer in air at 800 °C or freshly cleaved mica substrates by a drop-casting method. The cleaved mica was treated with UV ozone before coated with the samples. The crystalline structure of samples was characterized by X-ray diffraction (XRD, PANalytical Aeris) in the 2θ range of 5–40°. The operating tube current and voltage were 30 mA and 40 kV, respectively. The elemental analysis was conducted using X-ray photoelectron spectroscopy (XPS, JEOL JPS-9030) with a pass energy of 20 eV. Energy dispersive spectroscopy (EDS) was performed using JSM-IT 100 LA.

Electrochemical characterization

All electrochemical measurements were carried out with an electrochemical working station (Solartron SI1287) at room temperature in an open three-electrode cell system. The modified glassy carbon electrode (ϕ = 3 mm) was used as the working electrode. A platinum wire and Ag/AgCl were used as a counter electrode and a reference electrode, respectively. Electrode material (20 mg) in NMP (1 mL) was sonicated to make uniform dispersion. 2 μL of the dispersion was taken up using a pipet gun, dropped onto the glassy carbon electrode (ϕ = 3 mm), and dried at 50°C for 1 h under vacuum, then it was used

as a working electrode. The electrochemical performance was measured in a potential range of 0-1 V, with a scan rate of 50 mVs^{-1}. All electrochemical experiments were performed in 0.5 M H_2SO_4 aqueous electrolyte. The electrochemical impedance test was conducted at a frequency range of 100 kHz to 0.01 Hz at 0.4 V with an AC perturbation of 5 mV. The specific capacitance of the supercapacitor (C ($F g^{-1}$)) was calculated from the discharge curve according to the following formula:

$$C = \frac{I \times \Delta t}{m \times \Delta V}$$

where I is the constant current in discharging, m is the mass of active material on working electrode, Δt is the discharge time, and ΔV is the voltage change during discharge.

Results and Discussion

Our strategy to synthesize a graphene–polymer composite with a linker (**GO 3**) involved three steps: (1) functionalization of graphene with 1,3-diaminopropane to obtain **GO 1**; (2) addition of a monomer (*N,N'*-bissulphinyl-*m*-benzenediamine) to **GO 1** to obtain **GO 2**; (3) addition of another monomer (1,4-phenylenediamine) to **GO 2** to initiate polymerization (Scheme 2). The amine functionalization of GO [26] and the polymer synthesis [25] were independently reported, and we prepared **GO 1**, **GO 2**, and **GO 3** following these previous reports. Possible side reactions, such as neutralization of amine and *N,N'*-bissulphinyl-*m*-benzenediamine with acidic functional groups on GO were observed (Fig. S1a and Scheme S2). But, the side reactions were not shown in the structure of **GO 3** for simplicity.

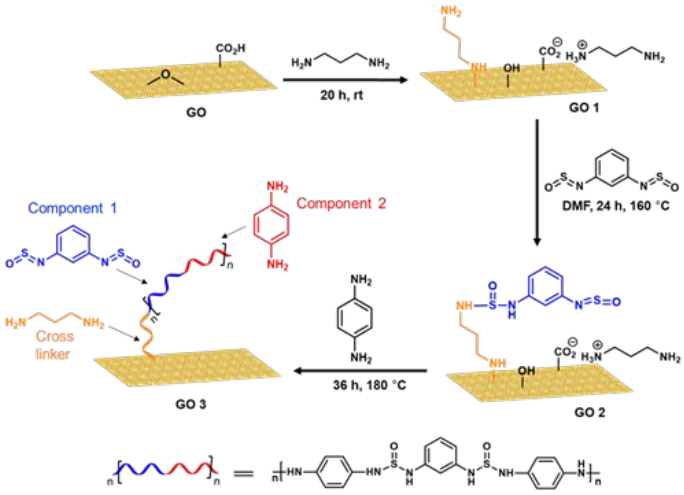

Scheme 2. Synthetic route for producing **GO 3**.

Characterization

The structure of the products was confirmed using X-ray photoelectron spectroscopy (XPS), thermogravimetric analysis (TGA), Fourier-transform infrared (FTIR), atomic force microscopy (AFM), and scanning electron microscopy (SEM). Initially, the elemental compositions of **GO 1**, **GO 2**, and **GO 3** were analyzed using XPS (Fig. 1a). Survey XPS spectra of **GO 1** showed the presence of nitrogen, which confirmed the functionalization of GO with 1,3-diaminopropane (Fig. 1ai) [27]. The XPS analysis of **GO 2** showed the presence of nitrogen and sulfur, which confirmed the functionalization of the initiation site (Fig. 1aii). Analysis of the XPS spectra showed the amount of N and S in **GO 2** was 4.1% and 1.2%, respectively; after polymerization, the amount of N and S was increased to 6.5% and 1.6%, respectively (Fig. 1aiii). The greater amount of N and S in **GO 3** compared with **GO 2** confirms the progress of the polymerization. The amount of oxygen in **GO 1**, **GO 2**, and **GO 3** was 25.6%, 17.5%, and 11.0%, respectively (Table S1). The smaller amount of oxygen in **GO 3** suggested reduction of GO occurred during heating. To gain further insight into the chemical composition, each element was analyzed using narrow-scan XPS (Fig. S1). The spectrum of **GO 1** showed a peak at 399.5 eV in the N 1s region, which suggested the formation of a covalent C–N bond [28], and confirmed the functionalization of GO with 1,3-diaminopropane. Similarly, a new peak was observed in the S 2p region of **GO 3** at 163.5 eV, which could be attributed to a C–S=O bond from the polymer [29]. These spectral changes indicate the successful grafting of the polymer onto graphene.

Next, the thermal stability of each material was measured using TGA (Fig. 1b). The TGA curve of GO showed that most weight loss occurred below 150°C in the N_2 atmosphere, which was due to the removal of adsorbed water and oxygen-containing groups (Fig. 1bi) [30]. In the case of **GO 1**, a slow weight loss was observed, starting from 150–250°C, due to the thermal decomposition of remaining oxygenated functional groups and 1,3-diaminopropane [31], from the GO (Fig. 1bii). The lower weight loss observed in **GO 1** compared with GO could be attributed to the partial reduction of GO by diamine, as reported previously [32]. The TGA curve of the pristine polymer suggested that the polymer decomposed only gradually above 250°C, with almost 50 wt% remaining even at 850°C (Fig. 1biii). Comparing the TGA curve of **GO 3** with these data, the weight loss between 150°C and 200°C could be ascribed to the removal of oxygen functional groups and 1,3-diaminopropane from GO, and the weight loss between 300°C and 400°C could be attributed to the decomposition of the polymer. Both of these observations suggest that the polymer was successfully cross-linked to the graphene in **GO 3** (Fig. 1biv).

The FTIR spectrum of GO (Fig. 1ci) revealed the presence of O–H (3435 cm^{-1}), C=O (1735 cm^{-1}), C=C (1615 cm^{-1}), and C–O (1052 cm^{-1}) functional groups [33]. The FTIR spectrum of **GO 1** exhibited a peak at 2900 cm^{-1}, which was attributed to the alkyl chain of 1,3-diaminopropane (Fig. 1cii) [34]. The spectrum **GO 2** contained a small peak corresponding to S=O at 1430 cm^{-1}, and the intensity of this peak was greater in the FTIR spectra of the pristine polymer [25], and **GO 3**.

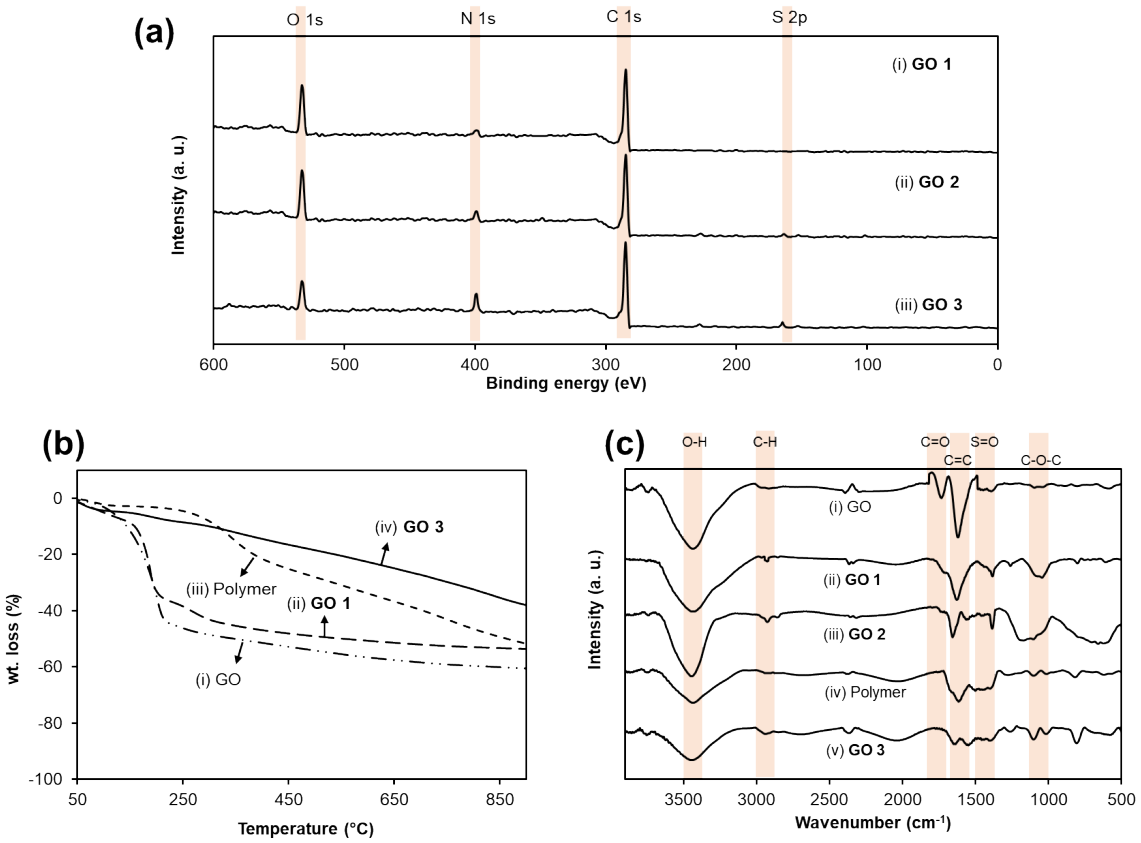

Fig. 1. (a) Wide-scan X-ray photoelectron spectra of (i) **GO 1**, (ii) **GO 2**, and (iii) **GO 3**. (b) Thermogravimetric analysis of (i) GO, (ii) **GO 1**, (iii) polymer, and (iii) **GO 3**. (c) Fourier-transform infrared analysis of (i) GO**,** (ii) **GO 1,** (iii**) GO 2,** (iv) polymer, and (v) **GO 3**.

The stepwise functionalization of graphene was confirmed by AFM (Fig. 2). The average height of GO was approximately 0.9 nm (Fig. 2a). The height of a **GO 1** and **GO 2** was 1.3 nm and 1.5 nm, respectively. The values are only slightly larger than that of the pristine GO (Fig. 2b); therefore, we consider 1,3-diaminopropane and/or *N,N′*-bissulphinyl-*m*-benzenediamine are bent or almost horizontal to GO plane. The height of **GO 3** was about 16 nm, much higher than others, due to the growth of polymer on graphene (Fig. 2d). This dramatic increase in the surface height of **GO 3** proves the bonding of the polymer on the surface of graphene.

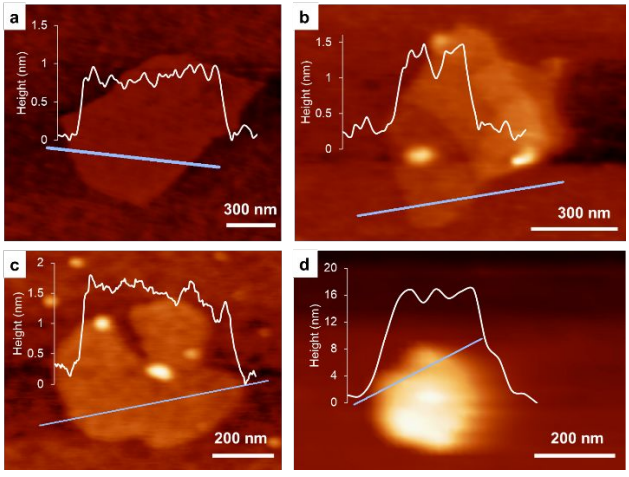

Fig. 2. Atomic force microscope image analysis of (a) GO, (b) **GO 1**, (c) **GO 2**, and (d) **GO 3**.

The morphologies of GO, **GO 1**, **GO 2**, and **GO 3** were further analyzed using SEM, which indicated that GO consisted of thin single-layer sheets (Fig. 3a), and that these structures were retained by **GO 1** (Fig. 3b) and **GO 2** (Fig. 3c) after their functionalization. These observations were consistent with the AFM analyses. The SEM image of **GO 3** showed a spherical shape (Fig. 3d), possibly because of the uniform growth and encapsulation of the graphene by the polymer. GO is negatively charged, and the nitrogen groups on polymer would be positively charged; therefore, ionic interaction would occur. The SEM images showed good agreement with AFM images.

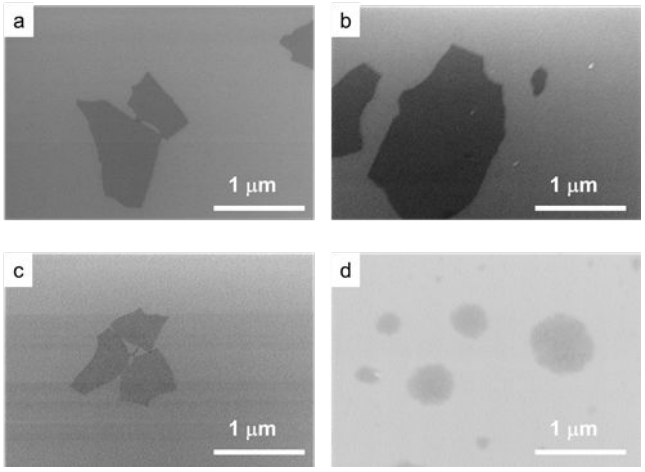

Fig. 3. Scanning electron microscope images of (a) GO, (b) **GO 1** and (c) **GO 2,** (d) **GO 3**.

Electrochemical performance as a supercapacitor

Cyclic voltammetry (CV) is an effective method to determine pseudocapacitive performance. The CV curve of **GO 3** (Fig. 4 ai) showed a peak that may be attributed to the pseudocapacitance of the polymer. **GO 3** displayed excellent electrochemical performance, possibly resulting from the larger surface area associated with the uniform polymer distribution on the graphene. Secondly, the high performance of **GO 3** might be due to the synergistic effect of pseudocapacitance and EDLC, which contribute to the overall capacitance.

The CV curve of non-crosslinked graphene–polymer mixture showed lower electrochemical performance than **GO 3** (Fig. 4 aii). Graphene cannot maintain a single-layer structure in the solid-state due to strong π–π interactions; therefore, a uniform composite with the polymer cannot be formed. This result suggests the layer-by-layer functionalization of GO, as shown by the AFM analysis, is essential for efficient electrochemical performance. The CV curve of the polymer showed redox peaks, but the electrochemical performance was low, possibly resulting from poor contact with the electrode due to polymer aggregation (Fig. 4 aiii). The CV curve of graphene (Fig. 4 aiv) showed a rectangular-like shape without redox peaks, indicating ideal EDLC behavior. The electrochemical performance of graphene is much lower than **GO 3**. The CV curve of **GO 3** composites is much larger than that of the pure polymer, pure graphene, and non-crosslinked graphene-polymer mixture, indicating higher specific capacitance. We believe that this drastic increase of total capacitance depends not only on the amplification effect of the pseudocapacitance by the polymer, but also on the amplification effect of EDLC due to the prevention of the stacking of graphene aided by the polymer.

When the CV curves of **GO 3** were acquired using different scan rates, all the curves maintained their shape (Fig. 4b), which indicated the stable supercapacitor behavior of **GO 3**. Fig. 4c represents the rate capability of **GO 3,** non-crosslinked graphene–polymer mixture, graphene, and polymer. With increasing current density, the capacitance of **GO 3** initially decreased before becoming stable. The capacitance of **GO 3** reached 172 F g^{-1} at 10 A g^{-1}, which is approximately 63% of its capacitance at 1 A g^{-1} (272 F g^{-1}) (Fig. 4c i). The specific capacitance of the non-crosslinked sample was 127 F g^{-1} at 10 A g^{-1}, which is 62% of its capacitance at 1 A g^{-1} (205 F g^{-1}) (Fig. 4c ii). Pure polymer and graphene composite electrodes can only deliver a specific capacitance of 30 F g^{-1} and 40 F g^{-1}, respectively, at a current density of 1 A g^{-1}, which decreased with increasing current density (Fig. 4c (iii and iv)). However, **GO 3** demonstrated high capacitance due to the combined effect of polymer (pseudocapacitance) and isolated graphene (EDLC), which allows fast transport of electrolyte ion. The capacitances of all samples were calculated after five cycles. To comprehensively understand the capacitive response of **GO 3**, an electrochemical impedance test was conducted as shown in Fig. S7. The nearly vertical arm of the AC impedance in the low-frequency region indicates an excellent capacitive behavior, representative of fast ion diffusion and adsorption in or on the

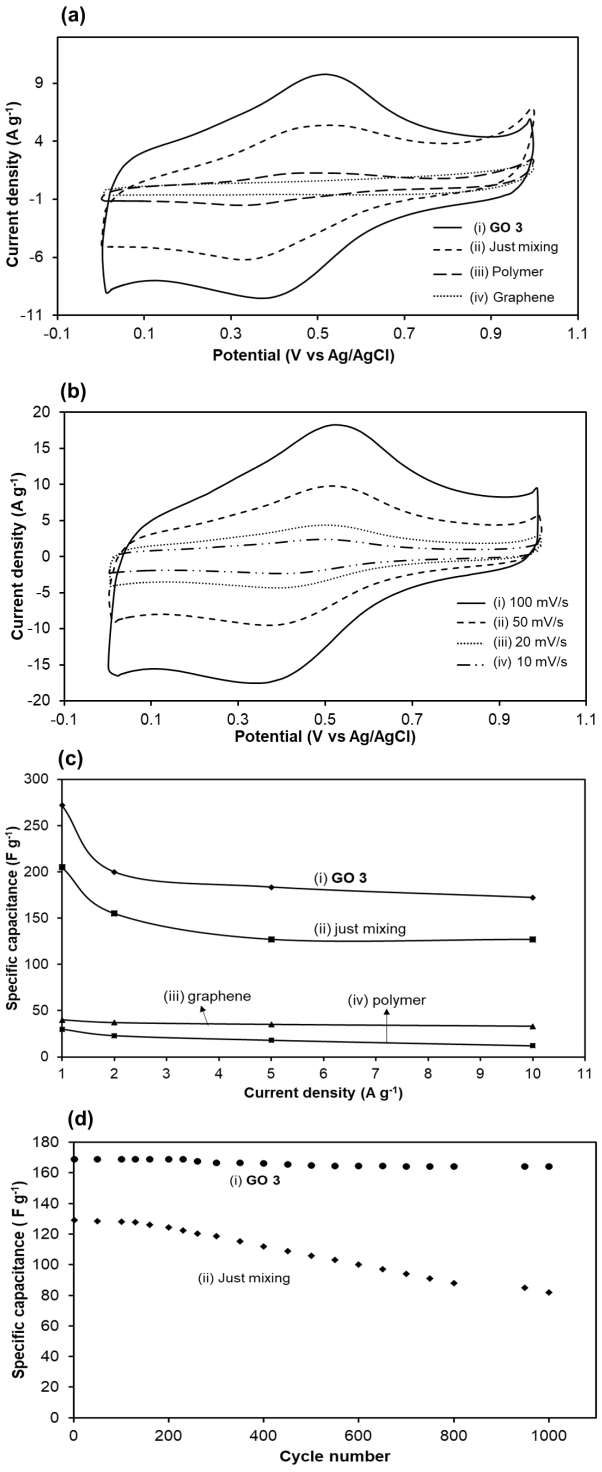

Fig. 4. Electrochemical evaluation of a three-electrode system using a scan rate of 50 mV s^{-1}. (a) Cyclic voltammograms of (i) **GO 3**, (ii) just mixing, (iii) polymer, and (iv) graphene. (b) Cyclic voltammograms of **GO 3** at different scan rates. (c) Specific capacitance of (i) **GO 3**, (ii) just mixing (non-crossed linked polymer-graphene), (iii) graphene, and (iv) polymer as a function of current density. (d) Cycling stability of (i) **GO 3** and (ii) just mixing sample using a current density of 10 A g^{-1}.

electrode material. The low resistance and fast ion diffusion can be attributed to the uniform distribution of polymer on graphene connected by covalent bond through cross-linker, which renders **GO 3** promising as a supercapacitor electrode. Fig. S8 indicates the galvanostatic charge/discharge tests at a current density of 0.5, 1, 2, 5, and 10 A g^{-1}. The nonlinear charge/discharge curves indicate the pseudocapacitive behavior of the polymer in **GO 3**.

Measurements of the cycling stability of **GO 3** during repeated charge/discharge cycles (Fig. 4di) showed that its specific capacitance remained approximately 98% of its initial capacitance after 1000 cycles with a constant current density of 10 A g^{-1}. Thus, **GO 3** showed good cycling stability in comparison with previous reports (Table S4). This illustrates that **GO 3** possesses good stability, a long lifetime, and a high degree of reversibility during repetitive charge/discharge cycling. In comparison, the non-crosslinked graphene–polymer mixture displayed a lower capacitance that continuously decreased during several hundred cycles (Fig. 4dii), its capacitance retention being 63% after 1000 cycles. The high capacitance and good cycling stability of **GO 3** can be attributed to the strong covalent connection between polymer and graphene and its uniform distribution on the graphene surface, allowing fast transport of electrolyte ions. Finally, we investigated the capacitive and diffusion-controlled contribution to the whole capacitance of **GO 3**. As a result, the ratios of capacitive/diffusion-controlled contributions were 4.5-1.6, suggesting the success of our strategy to fully utilize the EDLC and pseudocapacitance of **GO 3** (Table S5).

Conclusion

GO was functionalized with a polymer using simple mixing and heating, without the addition of a catalyst, acid, or oxidant. The graphene–polymer composite **GO 3** was prepared using a sequential three-step reaction. Structural analyses showed that the polymer and the graphene were cross-linked by a strong covalent bond. Polymer particles are uniformly wrapped within or on the surface of graphene. The electrical properties of the composite were evaluated to determine its suitability as an electrode material for a supercapacitor. **GO 3** demonstrated a high capacitance (272 F g-1 for **GO 3** vs. 205 F g-1 for the non-crosslinked graphene–polymer mixture at 1 A g-1) and good cycling stability (98% @ 1000 cycles for **GO 3** vs. 63% for the non-crosslinked graphene–polymer mixture at 10 A g-1). The superior electrochemical performance of **GO 3** is proposed due to the synergistic interaction of the polymer and graphene, allowing for fast electron transfer. This method of functionalization can be used for the future preparation of another graphene–polymer-based composites.

Conflicts of interest

There are no conflicts to declare.

Acknowledgements

We are grateful to Ms. Tomoko Ohkubo, Seiji Obata, Fumiko Tamagawa, and Benoit Campeon (Research Core for Interdisciplinary Sciences, Okayama University, Japan) for their help with the instrumentation facilities. This research was supported by JSPS KAKENHI (19H02718) and JST CREST (JPMJCR18R3).

Notes and references

1 Y. Wang, Z. Shi, Y. Huang, Y. Ma, C. Wang, M. Chen, Y, *J. Phys. Chem. C.* 2009, **113**, 13103.
2 C. Liu, Z. Yu, D. Neff, A. Zhamu, B. Z. Jang, *Nano Lett.* 2010, **10**, 4863.
3 K. Zhang, L. L. Zhang, X. S. Zhao, J. Wu, *Chem. Mater.* 2010, **22**, 1392.
4 H. Yang, S. Kannappan, A. Pandian, J.-H. Jang, Y. Lee, W. Lu, Nanotechnology 2017, **28**, 445401.
5 F. Zhang, T. Zhang, X. Yang, L. Zhang, K. Leng, Y. Huang, Y. Chen, *Energy Environ. Sci.* 2013, **6**, 1623.
6 D. Dutta, J. Y. Jiang, A. Jamaluddin, S. M. He, Y. H. Hung, F. Chen, J. K. Chang, C. Y. Su, *ACS Appl. Mater. Inter.* 2019, **11**, 36560.
7 A. Khosrozadeh, G. Singh, Q. Wang, G. Luo, M. Xing, *J. Mater. Chem. A*. 2018, **6**, 21064.
8 S. Ahmed, A. Ahmed, M. Rafat, *J. Saudi Chem. Soc.* 2018, **22**, 993.
9 W. Ma, S. Chen, S. Yang, M. Zhu, *RSC Adv.* 2016, **6**, 50112.
10 T. Nguyen, M. de F. Montemor, *Adv. Sci.* 2019, 6, 1801797.
11 G. A. Snook, P. Kao, A. S. Best, *J. Power Sources* 2011, **196**, 1.
12 S. Drieschner, M. Weber, J. Wohlketzetter, J. Vieten, E. Makrygiannis, B. M. Blaschke, V. Morandi, L. Colombo, F. Bonaccorso, J. A. Garrido, *2D Mater.* 2016, **3**, 045013.
13 A. Klechikov, G. Mercier, T. Sharifi, I. A. Baburin, G. Seifert, A. V. Talyzin, *Chem. Commun*. 2015, **51**, 15280.
14 Y. Qian, I. M. Ismail, A. Stein, *Carbon* 2014, **68**, 221.
15 H. Murata, Y. Nakajima, N. Saitoh, N. Yoshizawa, T. Suemasu, K. Toko, *Sci. Rep.* 2019, **9**, 4068.
16 M. A. Worsley, P. J. Pauzauskie, T. Y. Olson, J. Biener, J. H. Satcher, T. F. Baumann, *J. Am. Chem. Soc.* 2010, **132**, 14067.
17 D. G. Papageorgiou, I. A. Kinloch, R. J. Young, *Prog. Mater. Sci.* 2017, **90**, 75.
18 L. Liu, J. Zhang, J. Zhao, F. Liu, *Nanoscale* 2012, **4**, 5910.
19 S. Jo, Y. H. Park, S.-G. Ha, S. M. Kim, C. Song, S. Y. Park, I. In, *Synth. Met.* 2015, **209**, 60.
20 Z. Liu, H. Zhou, Z. Huang, W. Wang, F. Zeng, Y. Kuang, *J. Mater. Chem. A.* 2013, **1**, 3454.
21 Z. Gao, F. Wang, J. Chang, D. Wu, X. Wang, X. Wang, F. Xu, S. Gao, K. Jiang, *Electrochim. Acta* 2014, **133**, 325.
22 N. A. Kumar, H.-J. Choi, Y. R. Shin, D. W. Chang, L. Dai, J.-B. Baek, *ACS Nano* 2012, **6**, 1715.
23 L. Jianhua, A. Junwei, Z. Yecheng, M. Yuxiao, L. Mengliu, Y. Mei, L. Songmei, *ACS Appl. Mater. Interf.* 2012, **4**, 2870.
24 L. Lai, H. Yang, L. Wang, B. K. Teh, J. Zhong, H. Chou, L. Chen, W. Chen, Z. Shen, R.S. Ruoff, J. Lin, *ACS Nano* 2012, **6**, 5941.
25 N. A. El-Ghamaz, T. S. Ahmed, D. A. Salama, Eur. *Polym. J.* 2017, **93**, 8.
26 I. A. Vacchi, C. Spinato, J. Raya, A. Bianco, C. Menard-Moyon, *Nanoscale*, 2016, **8**, 13714.
27 B. Qian, C. Liu, J. Xu, Q. Sun, H. Yang, W. Liu, L. Zhang, T. Minari, X. Liu, J. Chen, *J. Phys. D: Appl. Phys.* 2019, **52**, 295502.
28 Z. Yang, Y. Dai, S. Wang, H. Cheng, J. Yu, *RSC Adv*. 2015, **5**, 78017.
29 D. Mhamane, S. Unni, A. Suryawanshi, O. Game, C. Rode, B.

Hannoyer, S. Kurungot, S. Ogale, activity, *J. Mater. Chem.* 2012, **22**, 11140.
30 C. C. Caliman, A. F. Mesquita, D. F. Cipriano, J. C. C. Freitas, A. a. C. Cotta, W. a. A. Macedo, A. O. Porto, *RSC Adv.* 2018, **8**, 6136.
31 J. Hu, B. He, J. Lu, L. Hong, J. Yuan, J. Song, L. Niu, *Int. J. Electrochem.* 2012, **7**, 10094.
32 Y. Gong, D. Li, Q. Fu, C. Pan, *Prog. Nat. Sci. Mater. Int.* 2015, **25**, 379.
33 H. Zare-Zardini, A. Taheri-Kafrani, A. Amiri, A.-K. Bordbar, *Sci Rep.* 2018, **8**, 586.
34 J. L. Yan, G. J. Chen, C. A. O. Jun, Y. Wei, B. H. Xie, M. B. Yang, *New Carbon Mater.* 2012, **27**, 370.